University of Groningen

Crystallization phenomena in germanium antimony phase-change films

Eising, Gert

IMPORTANT NOTE: You are advised to consult the publisher's version (publisher's PDF) if you wish to cite from it. Please check the document version below.

Document Version
Publisher's PDF, also known as Version of record

Publication date:
2013

Link to publication in University of Groningen/UMCG research database

Citation for published version (APA):
Eising, G. (2013). *Crystallization phenomena in germanium antimony phase-change films*. s.n.

Copyright
Other than for strictly personal use, it is not permitted to download or to forward/distribute the text or part of it without the consent of the author(s) and/or copyright holder(s), unless the work is under an open content license (like Creative Commons).

The publication may also be distributed here under the terms of Article 25fa of the Dutch Copyright Act, indicated by the "Taverne" license. More information can be found on the University of Groningen website: https://www.rug.nl/library/open-access/self-archiving-pure/taverne-amendment.

Take-down policy
If you believe that this document breaches copyright please contact us providing details, and we will remove access to the work immediately and investigate your claim.

Downloaded from the University of Groningen/UMCG research database (Pure): http://www.rug.nl/research/portal. For technical reasons the number of authors shown on this cover page is limited to 10 maximum.

Download date: 01-02-2024

Chapter 4

Laser accelerated crystallization

Abstract. For a proper understanding of crystallization kinetics it is preferred that isothermal studies are performed over a wide range of temperatures. However, such studies are generally confined to relatively low temperatures due to limitations in heating ramp rates, where crystallization should not start before the sample has become equilibrated at the desired isothermal temperature. For this reason the temperature range that could be studied in the previous chapter was relatively small, also because of the high activation energies for growth that hold for the studied phase-change materials. In the present chapter we extend the temperature range by applying laser-pulse heating in addition to isothermal heating of the phase-change film. We are able to optically study crystal growth at elevated temperatures not reachable using standard isothermal techniques. Still, laser pulses with durations of typically one second are used and this time is much longer than the time (less than 1 ms) required by the film to equilibrate at a certain laser-induced temperature. This way the crystal growth rates of several GeSb alloys are observed in a direct manner over six orders of magnitude. We find a non-Arrhenius temperature dependence for crystal growth and show that the growth can be well described based on a viscosity model incorporating the fragility of the supercooled liquid (glass) as an important parameter.

4.1 Introduction

Crystal growth in phase-change films is a temperature activated process. Methods for studying the crystal growth properties from room temperature up to and slightly above the glass-transition temperature are well established, and can be applied by, for example, placing a phase-change film on a hot plate or in a heating holder or furnace and using optical, atomic force or electron microscopy to study the crystal growth. [1, 2] Only microscopy-based techniques are able to directly determine crystal growth rates, because many other techniques like resistance measurements, differential scanning calorimetry, X-ray diffraction, etc. can be used to monitor the overall crystallized fraction, but cannot make a distinction between nucleation and growth. These techniques are generally also combined with isochronal (for a range of heating rates)

In preparation as *Laser Accelerated Isothermal Crystal Growth in Ge-Sb Phase-Change Films*, G. Eising, T. Van Damme, A Pauza and B. J. Kooi

instead of isothermal (for a range of temperatures) measurements making the analysis of the crystallization kinetics somewhat more approximate. Still, a drawback of isothermal measurements is that they generally limit the maximum growth rate that can be accurately measured in-situ (in our case for the optical method applied in the present thesis this is $\sim$5 μm s^{-1}). The reason for this limitations is mostly imposed by the (relatively slow) heating rates used to reach the isothermal temperature in combination with the requirement that crystallization only starts when the sample has become stabilized at the isothermal temperature.

In this chapter we will make an effort to optically observe crystal growth at higher temperatures, and thus higher growth rates, by using a laser to additionally heat the film and by monitoring the growth using a high speed camera. As explained, the benefit of optical microscopy over other methods to measure crystal growth at high temperatures, [3, 4] is that we can easily distinguish between the contribution of nucleation and growth. Moreover, phase-change materials are renowned for their excellent optical contrast between the amorphous and crystalline phase as exploited in rewritable optical disks (CD, DVD), making optical studies particularly suited. The assumption of Arrhenius-type growth behavior at temperatures higher than reachable with the standard isothermal experiments, like performed in chapter 3, will be tested. In order to do so, we still have to assume that we can measure isothermal crystal growth during the laser heating. This assumption holds, because (i) the duration of the laser pulse of the order of one second (where the laser reaches its set power level in $\sim$2 ns) is clearly longer than required by the sample to become equilibrated with respect to the laser heating (less than a ms) and (ii) we actually can measure (in a confined region) constant crystal growth velocities which is a clear indication of a constant temperature, because the growth rate is strongly temperature dependent.

4.2 Experimental

4.2.1 Samples

The samples used in this chapter consist of 200 nm thin films with a Ge_xSb_{100-x} composition (with $x = 6, 7, 8$ and 9) on a 1.3 mm thick glass substrate. The films were deposited and further processed as described in section 2.1.

4.2.2 Setup

Additional heating in the sample during isothermal heating was induced by focusing a 640 nm diode laser (Coherent Obis 640-100) with variable output power (40 to 110 mW) on the sample. The onset time to reach this power is less than 2 ns. The laser beam is at an incidence angle equal

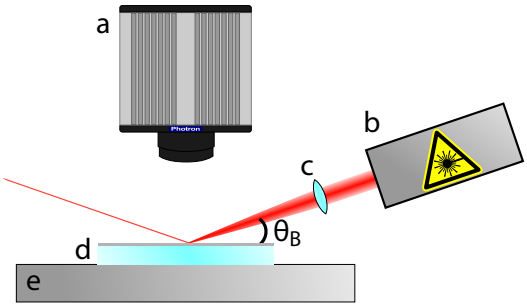

Figure 4.1 | Schematic overview of the laser setup. **a** High speed optical camera. **b** Diode laser. **c** Focusing optics. **d** Sample with a 200 nm thick GeSb film on a 1.3 mm thick glass substrate. **e** Ceramic heater. The angle between the incident laser and the sample surface should be close to the Brewster's angle, guaranteeing a maximum absorption in the film and minimum reflection.

to Brewster's angle θ_B (≈13° for the used films) [5] to minimize the reflection of the laser on the film, [6] see Fig. 4.1. Due to the angle, the circular laser beam creates a spot on the film with an elliptical shape with radii of $a \approx 250\,\mu m$ and $b \approx 110\,\mu m$ (spot size 1). By using different optics a second, larger, spot size was created with radii of $a \approx 1000\,\mu m$ and $b \approx 440\,\mu m$ (spot size 2). Optical recordings of the film were taken using a Photron 1024 PCI high speed camera, capable of recording up to 100 000 frames per second (fps). However, due to the limited resolution available at the maximum frame rate, we used recording rates of 1000 fps with a resolution of 1024×1024 pixels and 3000 fps with a resolution of 512×512 pixels. The duration of the laser pulse was 1 to 1.4 s. This duration was long enough to obtain a constant growth rate around the center of the laser spot.

4.2.3 Image analysis

The recordings were analyzed using line profiles as outlined in section 2.3 due to the local nature of the temperature increase. Additionally, the laser spot has a Gaussian power profile and therefore the crystal growth rates were determined around the center of the laser spot parallel to the long axis of the elliptical laser spot.

4.2.4 Local temperature estimation

An important part of the performed experiment is the determination of the local temperature at the laser spot. Direct measurement of the temperature proves to be difficult and therefore, we use an estimation of the temperature. For this, we assume that the crystal growth in the Ge_6Sb_{94} films shows Arrhenius behavior and follows the fit obtained in chapter 3 also in the

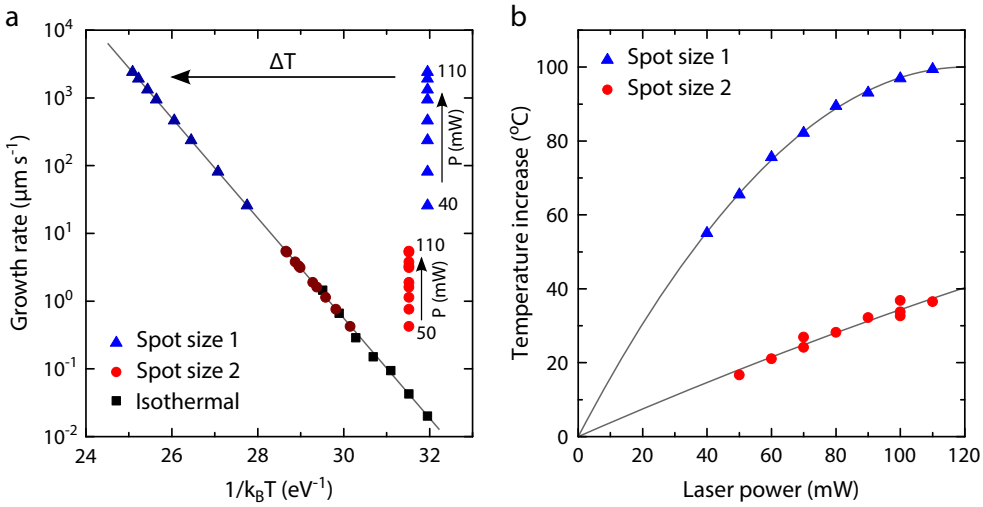

Figure 4.2 | Calibration of the temperature increase for given laser power. **a** Growth rate as function of laser power. By assuming Arrhenius-type growth behavior (gray line) for the Ge_6Sb_{94} alloy film, the temperature increase ΔT due to the laser pulse is determined. **b** Temperature differences, as determined based on the method in **a**, are plotted against laser power.

temperature range used in this chapter. As we will explain later, there is a good reason to make this assumption. In this way we can calculate the local temperature once we measure the crystal growth rate, see Fig 4.2. The growth rates are measured for different laser powers with the substrate at a fixed temperature of 90 °C (spot size 1) or 95 °C (spot size 2), see Fig. 4.2a. Using the Arrhenius fit obtained from isothermal experiments the temperature increase due to the laser pulse is determined (ΔT in Fig. 4.2a) and plotted as function of the laser power, see Fig. 4.2b. This was done for both spot sizes. For spot size 2 we find a nearly linear relation between the temperature increase and the laser power. For spot size 1 we find a decrease in the slope. This is attributed to increased heat dissipation due to an increased temperature difference with the surroundings. Second-order polynomial fits are used to interpolate the temperature increase. It is noted that, for laser-heating temperatures significantly higher than the temperature at which the calibrations were performed, the temperature increase for a given laser power is reduced (due to an increasing temperature difference with the surrounding and thus an increasing energy dissipation). The calibration thus provides an upper boundary of the temperature increase due to laser heating, whereas the extrapolation of the Arrhenius fit from the lower temperature region without laser heating (to higher temperatures) provides a lower boundary.

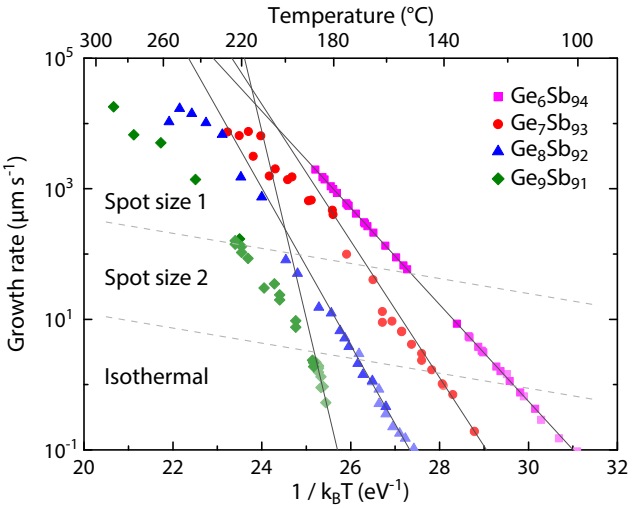

Figure 4.3 | Local crystal growth rates for standard isothermal heating with additional laser heating for compositions Ge_6Sb_{94} to Ge_9Sb_{91} versus the reciprocal temperature. Using the small spot size (spot size 1) the highest crystal growth rates are obtained. The standard isothermal results without laser heating are also included for reference, where the Arrhenius fits to these data are shown as (thin) solid black lines.

4.3 Results and discussion

The obtained crystal growth rates for the different alloys for both laser spot sizes together with the standard results from chapter 3 are shown in Fig. 4.3. With these standard isothermal experiments crystal growth rates up to ~5 µm s^{-1} could be obtained. Growth rates of up to ~20 mm s^{-1}, i.e., 4000 times faster, are reached using the smallest laser spot size. The Ge_6Sb_{94} films show, by assumption, no deviation from the isothermal fit. For Ge_7Sb_{93} and Ge_8Sb_{92} we initially see that the data points are following the isothermal Arrhenius fit, but at higher temperatures the growth rate becomes lower than expected from extrapolating the Arrhenius fit. For Ge_9Sb_{91} this deviation is already observed at ~10 µm s^{-1}. The change in slope of growth rate indicates a temperature dependence of the activation energy for growth.

The Arrhenius fits obtained from the crystal growth rates below 10 µm s^{-1} show, when extrapolated to higher temperatures, that Ge_9Sb_{91} reaches higher crystal growth rates than Ge_6Sb_{94} (see Fig. 4.3). This is unexpected behavior, because it is well-established that GeSb alloys with a higher antimony concentration show higher maximum crystallization speeds. [7] This indicates that the slope of the measured growth rates of Ge_9Sb_{91} has to decrease at higher temperatures to lower the crystal growth rates (compared to the Arrhenius fit extrapolated from

the region with growth rates below 10 μm s^{-1}) such that they remain below the crystal growth rates of Ge_8Sb_{92}, which in turn should remain below the ones of Ge_7Sb_{93} and Ge_6Sb_{94}. Indeed, by applying our method to determine the temperature increase due to laser heating, we measure crystal growth rates showing this natural evolution with the ones of Ge_9Sb_{91} remaining below Ge_8Sb_{92}, etc. (see Fig. 4.3). In this way Ge_9Sb_{91} shows most pronounced non-Arrhenius behavior, whereas Ge_6Sb_{94} has to show most pronounced Arrhenius behavior. Actually, this is also our justification for making the explicit assumption that Ge_6Sb_{94} keeps its Arrhenius behavior also during laser heating. Otherwise we were not able to estimate the temperature increase due to laser heating. This whole scheme seems like a circle reasoning, but the combined results in Fig. 4.3 for the various GeSb alloys show that there is in principle no alternative solution, i.e., the result has to be that Ge_9Sb_{91} shows most pronounced non-Arrhenius behavior, whereas Ge_6Sb_{94} has to show most pronounced Arrhenius behavior. Interesting to note is that only in the last few years crystal growth rates at sufficiently different temperatures have been determined for phase-change films (although generally indirectly), such that non-Arrhenius behavior could be established. [3, 8] In this respect, the result for Ge_9Sb_{91} is not unexpected, but it is the first microscopy-based result, where crystal growth has been measured directly and shows non-Arrhenius behavior. On the other hand, very recently a smart method was demonstrated, showing that the crystal growth rate for the AgInSbTe phase-change material (that is also a well-known fast-growth-type PCM, like our GeSb alloys) follows strict Arrhenius behavior for over eight orders of magnitude (from ∼10 nm s^{-1} to ∼1 m s^{-1}). [4] In this respect, the assumption that Ge_6Sb_{94} follows strict Arrhenius behavior between 100 nm s^{-1} and 3 mm s^{-1} (over four orders of magnitude) is also certainly possible.

4.3.1 Viscosity and fragility

Recently, interesting work has been done on studying the crystal growth rate, viscosity, and coupled, the fragility of phase-change materials at high temperatures, relevant to phase-change memory applications. [3, 4] Using Flash Differential Scanning Calorimeter (DSC) Orava et al. studied the widely used, nucleation-dominated, phase-change material $Ge_2Sb_2Te_5$ over a large temperature range, making it possible to study the crystallization at high crystal growth rates. [3] The downside of using this method is that several assumptions were needed to extract the crystal growth rates from the DSC measurements, where it is particularly difficult to distinguish between the contribution of nucleation and growth. However, they showed nicely that using the new Flash DSC technique it is well possible to study a phase-change material at high temperatures and that $Ge_2Sb_2Te_5$ exhibits a strongly non-Arrhenius growth dependence and high fragility above the glass transition temperature. [3] A more direct approach was done

by Salinga et al. using laser-based time-resolved reflectivity measurements. [4] They showed that the fast-growth material AgInSbTe exhibits a strong Arrhenius behavior over eight order of magnitude, also close to the maximum growth rate. Their whole analysis indicated that AgInSbTe should have an extremely high fragility. Both articles derive the viscosity from the measurement data to study the crystallization properties near the melting temperature.

To calculate the viscosity $\eta(T)$ from the crystal growth rate $u(T)$ we use the following equation: [4, 9]

$$\eta(T) = \frac{4 r_{\text{atom}} k_{\text{B}} T}{3\pi\lambda^2 R_{\text{hyd}} u(T)} \left(1 - \exp\left(-\frac{\Delta G(T)}{k_{\text{B}} T}\right)\right) \tag{4.1}$$

with r_{atom} the atomic radius (∼1.5 Å), λ the diffusional jump distance (∼1 Å), R_{hyd} the hydrodynamic radius (∼0.5 Å) and k_{B} the Boltzmann constant. These values are based on those reported for AgInSbTe. [4] The Thomson-Spaepen approximation is used to estimate the gain in Gibbs free energy $\Delta G(T)$: [10]

$$\Delta G(T) = \Delta H_{\text{m}} \frac{T_{\text{m}} - T}{T_{\text{m}}} \left(\frac{2T}{T_{\text{m}} + T}\right) \tag{4.2}$$

with ΔH_{m} the heat of fusion (∼0.22 eV at^{-1}) [11] and T_{m} the melting temperature (∼882 K for Ge_8Sb_{92} and ∼878 K for Ge_9Sb_{91}). [12]

The viscosity of glass-forming liquids can be modeled by: [13]

$$\log_{10}\eta(T) = \log_{10}\eta_\infty + (12 - \log_{10}\eta_\infty)\frac{T_{\text{g}}}{T} \exp\left[\left(\frac{m}{12 - \log_{10}\eta_\infty} - 1\right)\left(\frac{T_{\text{g}}}{T} - 1\right)\right] \tag{4.3}$$

with η_∞ the infinite temperature viscosity ($\log_{10}\eta_\infty \approx -3$), T_g the glass transition temperature and m the fragility.

The crystal growth rates measured for Ge_8Sb_{92} and Ge_9Sb_{91}, shown in Fig. 4.3, were used to calculate the viscosity as function of temperature using Eq. (4.1). The results are shown in Fig. 4.4. Using the model proposed by Mauro et al. (Eq. (4.3)) the data is fitted and the fragility m is obtained for both alloys. For Ge_8Sb_{92} $m \approx 61$ and $m \approx 59$ for Ge_9Sb_{91}. To obtain a good fit the glass transition temperature was set to ∼382 K for Ge_8Sb_{92} and ∼395 K for Ge_9Sb_{91}.

Compared with AgInSbTe [4] and $Ge_2Sb_2Te_5$ [3] the fragility is significantly lower, indicating that these GeSb alloys are a stronger liquid than $Ge_2Sb_2Te_5$ and AgInSbTe. No literature data could be found for the T_{g} of Ge_8Sb_{92} and Ge_9Sb_{91}. Comparing with $Ge_{12}Sb_{88}$, for which a T_{g} of ∼466 K has been reported, [11] the obtained values seem plausible.

4.3.2 Extrapolating crystal growth rates

The popular Arrhenius model, also applied in this thesis, is often not valid for the entire temperature regime of interest for a specific material. As shown in Fig. 4.3, if Arrhenius-type

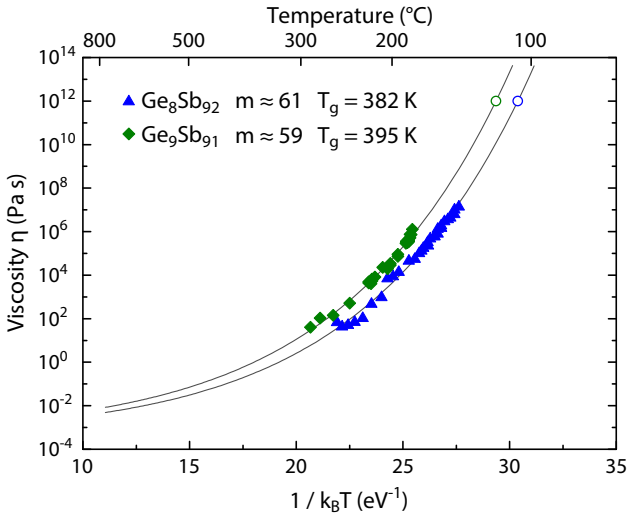

Figure 4.4 | Viscosity as function of reciprocal temperature for Ge_8Sb_{92} (blue symbols) and Ge_9Sb_{91} (green symbols). Using Eq. (4.1) the viscosity is calculated from the crystal growth rates as shown in Fig. 4.3 (diamond and triangles). The viscosity is fitted with Eq. (4.3) (gray solid lines). The glass transition temperatures obtained from the fits for Ge_8Sb_{92} and Ge_9Sb_{91} are ∼382 K and ∼395 K, respectively (open circles).

growth behavior would hold up to the melting temperature, Ge_9Sb_{91} should have a higher crystal growth rate at ∼200 °C than the other three measured GeSb compositions. From literature we expect a tendency that GeSb compositions with less germanium show higher maximum growth rates instead. [7] Indeed, using the laser induced crystallization measurements we do find non-Arrhenius growth behavior for crystal growth rates above the range probed with standard isothermal measurements. This does, however, mean that the growth rates cannot be extrapolated toward the melting temperatures, of interest for applications, using Arrhenius fits.

The viscosity model does give a good fit for the combined isothermal and laser measurements, and is therefore a good candidate model for extrapolating the crystal growth rates to higher temperatures. By reversing Eq. (4.1) and plugging in Eq. (4.3) with the parameters m and T_g obtained for Ge_8Sb_{92} and Ge_9Sb_{91} a prediction is made for the crystal growth rate at temperatures approaching the melting temperature and additionally maximum growth rates are found for both alloys (see Fig. 4.5). The maximum growth rate found in this way for Ge_8Sb_{92} is $u_{max} = 15\,m\,s^{-1}$.

The obtained maximum growth rate is lower than what could be expected from ref. [7] where a growth rate of ∼58 $m\,s^{-1}$ was measured for $Ge_{10}Sb_{90}$ films, which should have a lower maximum crystal growth rate due to the higher concentration of germanium. The experiments

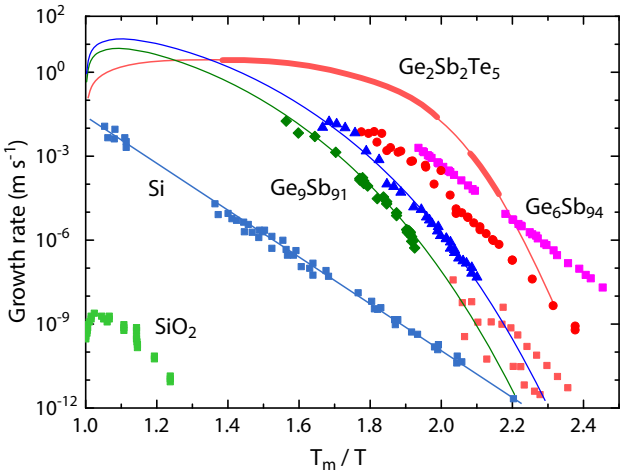

Figure 4.5 | Crystal growth rates a function of reciprocal temperature for different materials. The results for Ge_6Sb_{94} to Ge_9Sb_{91} obtained in the previous and current chapter are compared with the crystal growth rates for $Ge_2Sb_2Te_5$, Si and SiO_2. Like $Ge_2Sb_2Te_5$, the Ge_8Sb_{92} and Ge_9Sb_{91} alloys show fragile behavior. On the other hand, Si shows rather non-fragile behavior. The solid green and blue lines are the growth rates extracted from the viscosity fit by reversing Eq. (4.1) for Ge_8Sb_{92} and Ge_9Sb_{91}. The data for $Ge_2Sb_2Te_5$, Si and SiO_2 was adapted from [16].

present in ref. [7] were, however, done on melt-quenched films, whereas our experiments are done on as-deposited material. In general, a shift to a lower crystallization temperature can be expected when going from an as-deposited film to a melt-quenched film. For example, for $Ge_{15}Sb_{85}$ a decrease of 42 K has been reported. [14] Earlier work from our group for Ge and In doped SbTe alloys showed that the same crystal growth rates occurred at temperatures about 25 K lower for melt-quenched than for as-deposited materials. [15]. Such shifts to lower temperatures make it possible to reach, by our model, the maximum growth rate like the 58 m s^{-1} reported.

For phase-change materials it is desirable to have as high as possible maximum crystal growth rates allowing fast switching of the memory, but also crystal growth rates that become extremely slow at the maximum allowed operating temperature of the memory (like 100 °C) to give good data retention to the memory. Comparing the different materials in Fig. 4.5, these conflicting requirements seem to be best met by the Ge_8Sb_{92} and Ge_9Sb_{91} alloys. For the most popular phase-change material $Ge_2Sb_2Te_5$ it is indeed known that both its retention behavior and its switching speeds are rather modest, inspiring strong attempts to find materials with improved phase-change properties. Fig. 4.5 of course only shows a (small) part of the story, because for instance (i) it is known that GeSb alloys are more prone to phase separa-

tion than $Ge_2Sb_2Te_5$ and therefore cell endurance (cyclability) is clearly more an issue for the former alloys and (ii) the results for all the phase-change materials shown in Fig. 4.5 hold for as-deposited films and have limited value, because in practice always melt-quenched materials are used which generally show different behavior (e.g., lower crystallization temperature as explained above).

4.4 Conclusions

We have successfully demonstrated a method to optically study crystal growth rates at high temperatures, almost four orders of magnitude higher than reachable with previous standard isothermal measurements, by combining laser and isothermal heating with high speed optical microscopy. The local temperature increase due to the laser pulse was estimated providing an upper and lower bound for the temperature at a certain growth rate. After transposing the crystal growth rate versus temperature to the viscosity versus temperature a good fit was obtained for the fragile behavior of the viscosity ($m \approx 60$), also allowing for a prediction of the crystal growth rates with a certain maximum rate ($15\,\mathrm{m\,s^{-1}}$) at temperatures near the melting temperature.

References

[1] V. Weidenhof, I. Friedrich, S. Ziegler, M. Wuttig, *Journal of Applied Physics* **89**, 3168 (2001).

[2] B. J. Kooi, J. T. M. De Hosson, *Journal of Applied Physics* **95**, 4714 (2004).

[3] J. Orava, A. L. Greer, B. Gholipour, D. W. Hewak, C. E. Smith, *Nature Materials* **11**, 279 (2012).

[4] M. Salinga, E. Carria, A. Kaldenbach, M. Bornhöfft, J. Benke, J. Mayer, M. Wuttig, *Nature Communications* **4** (2013).

[5] D. Z. Dimitrov, C. Babevab, S.-T. Chenga, W.-C. Hsua, M.-H. Hsieha, S.-Y. Tsaia, High-speed reversible phase-change optical recording in GeSb – based alloys, *European\Phase Change and Ovonics Symposium* (2004).

[6] Brewster, D., *Philosophical Transactions of the Royal Society of London* (1815), vol. 105, pp. 125–159.

[7] D. J. Adelerhof, Media development for DVD+RW phase change recording, *European\Phase Change and Ovonics Symposium* (2004).

[8] N. Ciocchini, D. Ielmini, Crystallization phenomena in phase change memories: non-arrhenius kinetics, modeling and novel applications, *European\Phase Change and Ovonics Symposium* (2013).

[9] D. Turnbull, J. C. Fisher, *The Journal of Chemical Physics* **17**, 71 (1949).

[10] C. V. Thompson, F. Spaepen, *Acta Metallurgica* **27**, 1855 (1979).

[11] J. A. Kalb, Crystallization kinetics in antimony and tellurium alloys used for phase change recording, Ph.D. thesis, RWTH Aachen University, Aachen (2006).

[12] R. W. Olesinski, G. J. Abbaschian, *Bulletin of Alloy Phase Diagrams* **7**, 219 (1986).

[13] J. C. Mauro, Y. Yue, A. J. Ellison, P. K. Gupta, D. C. Allan, *Proceedings of the National Academy of Sciences* **106**, 19780 (2009). PMID: 19903878.

[14] L. van Pieterson, M. H. R. Lankhorst, M. van Schijndel, A. E. T. Kuiper, J. H. J. Roosen, *Journal of Applied Physics* **97**, 083520 (2005).

[15] J. L. Oosthoek, B. J. Kooi, J. T. De Hosson, D. J. Gravesteijn, K. Attenborough, R. A. Wolters, M. Verheijen, Crystallization studies of doped SbTe phase-change thin films and PRAM line cells: Growth rate determination by automated TEM image analysis, *European\Phase Change and Ovonics Symposium* (2009).

[16] M. Wuttig, M. Salinga, *Nature Materials* **11**, 270 (2012).